Monthly Notices
of the
ROYAL ASTRONOMICAL SOCIETY

MNRAS **430,** 996–1007 (2013) doi:10.1093/mnras/sts672

Five new outbursting AM CVn systems discovered by the Palomar Transient Factory

David Levitan,[1⋆] Thomas Kupfer,[2] Paul J. Groot,[1,2] Shrinivas R. Kulkarni,[1] Thomas A. Prince,[1] Gregory V. Simonian,[1] Iair Arcavi,[3] Joshua S. Bloom,[4] Russ Laher,[5] Peter E. Nugent,[4,6] Eran O. Ofek,[3] Branimir Sesar[1] and Jason Surace[5]

[1]*Division of Physics, Mathematics, and Astronomy, California Institute of Technology, Pasadena, CA 91125, USA*
[2]*Department of Astrophysics/IMAPP, Radboud University Nijmegen, PO Box 9010, NL-6500 GL Nijmegen, the Netherlands*
[3]*Department of Particle Physics and Astrophysics, Weizmann Institute of Science, Rehovot 76100, Israel*
[4]*Department of Astronomy, University of California, Berkeley, CA 94720-3411, USA*
[5]*Spitzer Science Center, MS 314-6, California Institute of Technology, Pasadena, CA 91125, USA*
[6]*Computational Cosmology Center, Lawrence Berkeley National Laboratory, 1 Cyclotron Road, Berkeley, CA 94720, USA*

Accepted 2012 December 18. Received 2012 December 14; in original form 2012 September 18

ABSTRACT

We present five new outbursting AM CVn systems and one candidate discovered as part of an ongoing search for such systems using the Palomar Transient Factory (PTF). This is the first large-area, systematic search for AM CVn systems using only large-amplitude photometric variability to select candidates. Three of the confirmed systems and the candidate system were discovered as part of the PTF transient search. Two systems were found as part of a search for outbursts through the PTF photometric data base. We discuss the observed characteristics of each of these systems, including the orbital periods of two systems. We also consider the position of these systems, selected in a colour-independent survey, in colour–colour space and compare to systems selected solely by their colours. We find that the colours of our newly discovered systems do not differ significantly from those of previously known systems, but significant errors preclude a definitive answer.

Key words: accretion, accretion discs – binaries: close – stars: individual: PTF1 J043517.73+002940.7 – stars: individual: PTF1 J094329.59+102957.6 – novae, cataclysmic variables – white dwarfs.

1 INTRODUCTION

AM CVn systems are rare, ultracompact, semi-detached white dwarf (WD) binaries with periods ranging from 5 to 65 min. First proposed as a class of binary systems over 40 years ago by Smak (1967), fewer than 10 additional systems were discovered in the following 30 years. The availability of wide-area surveys – first photometric, then spectroscopic, and now synoptic – has resulted in the discovery of over 20 systems in just the last decade, yet their rich and complex phenomenological behaviour and evolutionary history has limited our understanding of these degenerate post-period minimum binaries. AM CVn systems are believed to be one possible outcome of double degenerate WD evolution, along with R CrB stars, massive single WDs, and Type Ia supernovae (Webbink 1984; Nelemans et al. 2001). They are extremely important as strong low-frequency Galactic gravitational wave sources (e.g. Nelemans, Yungelson & Portegies Zwart 2004; Roelofs, Nelemans & Groot 2007c; Nissanke et al. 2012) and are the source population of the proposed '.Ia' supernovae (Bildsten et al. 2007). However, the lack of an accurate population density has complicated their use for understanding these phenomena. We refer the reader to Nelemans (2005) and Solheim (2010) for general reviews.

The first 11 AM CVn systems were serendipitous discoveries. Several were initially of interest as supernova candidates (e.g. Jha et al. 1998; Wood-Vasey et al. 2003). The availability of the Sloan Digital Sky Survey (SDSS) and, specifically, its spectroscopic data base, led to the first systematic search for AM CVn systems and yielded seven new systems based on their distinctive helium emission lines and lack of hydrogen (Anderson et al. 2005, 2008; Roelofs et al. 2005). However, the SDSS spectroscopic data base is not complete and spectroscopic targets are selected based on complex colour criteria and fibre availability. Roelofs et al. (2009) noticed that the

⋆E-mail: dlevitan@caltech.edu

known AM CVn systems are clustered in a relatively sparse area of the colour–colour space and proposed a spectroscopic survey of all SDSS sources inside a predetermined colour cut. Although predictions of up to a total of 50 systems in the SDSS were made (based on Roelofs et al. 2007c), the survey, now wrapping up, has found fewer than 10 additional systems (Roelofs et al. 2009; Rau et al. 2010; Carter et al. 2013).

Although successful, such colour-selected spectroscopic surveys are both resource intensive and inherently biased to the previously known population. AM CVn systems have similar colours to other blue objects, including WDs [particularly DB (helium-line) WDs] and quasars. Expanding the colour selection to a wider box appears to offer a significant increase of the number of candidates with few gains in the number of discovered AM CVn systems. A way to further down-select candidates, or completely change the selection criteria, is thus necessary.

AM CVn systems are thought to have distinctly different phenomenology dependent on their orbital periods. Believed to be binaries hosting degenerate mass donors that have evolved through a period minimum, their orbital periods increase as angular momentum is lost to gravitational wave radiation. The most recently formed systems, with periods below ∼20 min, are in a constant state of high mass transfer from the donor to the optically-thick accretion disc. They have been referred to as 'high'-state systems and exhibit properties similar to dwarf nova cataclysmic variables (CVs) in outburst, including superhumps and absorption line spectra (e.g. Roelofs et al. 2006b, 2007b; Fontaine et al. 2011).

The oldest systems – those with orbital periods over ∼40 min and thus low mass transfer rates – are characterized by their lack of photometric variability and strong helium emission lines from the optically-thin disc. Spectroscopic surveys are primarily sensitive to systems with these emission lines.

Between these two extremes are the 'outbursting' systems, thought to have orbital periods between roughly 20 and 40 min. These systems are characterized by their changes between a high state and a low state, which results in both a luminosity change of 3–5 mag and (typically) a change in the spectral features from absorption lines to emission lines. In each state, they generally take on the properties of that state, with the significant addition of photometric variability in the low state for some of the systems. This variability was tied to the orbital period by Levitan et al. (2011), but any link between the photometric and spectroscopic variability remains to be confirmed by observations of additional systems. Outbursts typically last for a period of the order of days to weeks, and are recurrent on time-scales of a few months to over a year (Kato et al. 2000; Ramsay et al. 2012). Large-area synoptic surveys are most sensitive to these outbursting systems and the first system from such a survey was reported by Levitan et al. (2011) using the Palomar Transient Factory (PTF; Law et al. 2008).

In this paper, we continue the survey work started in Levitan et al. (2011) and report on the discovery of an additional five AM CVn systems and one faint candidate as part of the PTF AM CVn System Key Project. This search is the first systematic, large-area colour-independent search for AM CVn systems that relies solely on their large-amplitude, photometric variability to identify candidates.

We introduce the PTF in Section 2 and describe our AM CVn system detection strategy and data reduction processes. We report on our discoveries in Section 3, including both photometric measurements of the individual systems and period analysis based on phase-resolved spectroscopy. In Section 4, we discuss the features of these systems and compare their colours to the colour selection criterion used in the aforementioned spectroscopic survey.

2 SOURCE DETECTION AND ANALYSIS PROCESS

The PTF[1] uses the Samuel Oschin 48-arcsec Schmidt telescope at the Palomar Observatory to image up to ∼2000 deg^2 of the sky per night to a median depth on dark nights of $R \sim 20.6$ or $g' \sim 21.3$ (Law et al. 2008; Rau et al. 2009). The cadence of observations is not uniform and has varied from 90 s to 5 d, depending on the observational programme conducted at the time.

Two pipelines process PTF data. The 'transient' pipeline uses difference imaging for the rapid discovery of transient events. Exposures are automatically reduced and processed within a few hours of acquisition, and candidate events, identified using difference photometry, are analysed by both automated routines and humans (Law et al. 2008). Conversely, the 'photometric' pipeline is designed for accuracy, not speed. In this pipeline, exposures are processed after the end of the night using aperture photometry (Laher et al., in preparation). Instrumental magnitudes are calibrated to the SDSS, and instrumental effects, airmass and background are detrended (Ofek et al. 2012). Finally, light curves are generated using relative photometry algorithms (Levitan et al., in preparation). From this photometric data base, we select sources for follow-up observations. Most sources selected as part of this search were identified as CVs and are detailed in Groot et al. (in preparation).

We refer to the AM CVn systems presented in this paper as either 'transient' discovered or 'photometrically' discovered. The former are those initially selected as supernova candidates and classified as part of the PTF supernova search. 'Photometrically' identified systems were found by scanning through light curves for outbursts. These systems were selected by searching for outbursts of 2 mag above the median magnitude that have a second measurement at least 1 d later that is 5σ brighter than the median.

2.1 Data reduction procedures

All PTF light curves presented in this paper were processed through the photometric pipeline referred to earlier. The relative photometry algorithm used for the data in this paper (both PTF and targeted observations) is a matrix-based least-squares algorithm. The algorithm was described briefly in Ofek et al. (2011) and Levitan et al. (2011). Further details and the specific application to the PTF data will be found in Levitan et al. (in preparation). We note that the systematic uncertainty limit of the PTF relative photometry is approximately 6–8 mmag (based on bright stars with $14.5 < m_R < 16$). Errors of ∼0.1 mag are achieved at $m \sim 19$ and of ∼0.2 mag at $m \sim 21$.

The spectroscopic data were reduced using either standard IRAF tasks or using optimal extraction (Horne 1986) as implemented in the PAMELA code (Marsh 1989) as well as the Starlink packages KAPPA, FIGARO and CONVERT. The spectra acquired for the phase-resolved spectroscopy were all reduced using the latter. Spectra obtained from the red side of Keck-I/LRIS were processed with L.A. COSMIC (van Dokkum 2001) due to the large number of cosmic rays. Photometric data from the Palomar 200 arcsec (P200) and the Nordic Optical Telescope (NOT) were reduced using standard bias-subtraction and flat-fielding techniques. Point spread function photometry as implemented in either DAOPHOT or AUTOPHOTOM was

[1] http://www.astro.caltech.edu/ptf

Table 1. PTF-discovered AM CVn system properties.

System	Discovery pipeline	Period (min)	Outburst magnitude[a]	Quiescent magnitude u'	g'	r'	i'
PTF1 J043517.73+002940.7[b]	Transient[c]	34.31 ± 1.94	18.4 (R)	22.14 ± 0.11	22.28 ± 0.04	22.45 ± 0.04	22.60 ± 0.10
PTF1 J085724.27+072946.7	Transient[c]	...	19.5 (R)	21.68 ± 0.02	21.68 ± 0.01	21.74 ± 0.02	21.74 ± 0.04
PTF1 J094329.59+102957.6	Photometric	30.17 ± 0.65	16.9 (R)	20.51 ± 0.01	20.71 ± 0.01	21.09 ± 0.02	21.17 ± 0.05
PTF1 J152310.71+184558.2	Transient[c]	...	17.6 (R)	23.28 ± 0.12	23.48 ± 0.05	23.34 ± 0.06	23.14 ± 0.08
PTF1 J163239.39+351107.3[b, d]	Transient[c]	...	17.9 (g')	22.74 ± 0.14	22.99 ± 0.07	22.98 ± 0.06	...
PTF1 J221910.09+313523.1	Photometric	...	16.2 (g')	20.50 ± 0.03	20.66 ± 0.06	20.90 ± 0.03	20.94 ± 0.02
PTF1 J071912.13+485834.0[e]	Transient	26.77 ± 0.02	15.56 (g')	...	...	...	...

Note. Quiescent magnitudes are from P200/LFC images and are not dereddened.
[a]This is the brightest detection in PTF in either R or g' but is likely not the actual peak magnitude.
[b]Also identified as a CV candidate by the Catalina Real-Time Transient Survey (Drake et al. 2009): PTF1 J0435+0029 = CSS090219:043518+00294; PTF1 J1632+3511 = CSS110507:163239+351108.
[c]PTF transient names: PTF1 J0435+0029 = PTF11avm; PTF1 J0857+0729 = PTF11aab; PTF1 J1523+1856 = PTF10noc; PTF1 J1632+3511 = PTF11dkq.
[d]This is an AM CVn system candidate. See discussion in Section 3.5.
[e]Originally published in Levitan et al. (2011) (included here for reference as a PTF-discovered AM CVn system).

Table 2. Details of observations.

System	Setup	UT date	State	Gratings/grisms	Exposure time (s)
PTF1 J0435+0029	P200/DBSP	2011 March 10	Outburst	B: 600/4000, R: 158/7500	600
...	Keck-I/LRIS	2011 March 12	Outburst	B: 400/3400, R: 400/7500	800
...	Keck-I/LRIS	2011 March 26	Quiescence	B: 400/3400, R: 400/7500	1080
...	Keck-I/LRIS	2011 October 29[a]	Quiescence	B: 600/4000, R: 600/7500	180 s× 81
...	P200/LFC	2012 November 22	Quiescence	Imaging (u', g', r', i')	480, except u': 900
PTF1 J0857+0729	KPNO 4-m/RC	2011 February 1[a]	Outburst	316/4000	1800
...	NOT/ALFOSC	2011 February 2	Outburst	#11 (200/5200)	120
...	P200/LFC	2011 November 30	Quiescence	Imaging (g')	45 s× 80
...	NOT/ALFOSC	2012 February 28	Quiescence	Imaging (g')	60 s× 110
...	P200/LFC	2012 November 22	Quiescence	Imaging (u', g', r', i')	300, except u': 600
PTF1 J0943+1029	Keck-I/LRIS	2011 October 29	Quiescence	B: 600/4000, R: 600/7500	1200
...	Keck-I/LRIS	2011 December 25[a]	Quiescence	B: 600/4000, R: 600/7500	180 s× 80
...	Keck-I/LRIS	2011 December 31[a]	Quiescence	B: 600/4000, R: 600/7500	180 s× 25
...	P200/LFC	2012 November 22	Quiescence	Imaging (u', g', r', i')	300, except u': 600
PTF1 J1523+1845	Keck-I/LRIS	2010 July 7	Outburst	B: 400/3400, R: 400/7500	200
...	Keck-I/LRIS	2010 July 8[a]	Outburst	B: 400/3400, R: 400/7500	300
...	P200/LFC	2012 January 30	Quiescence	Image(u', g', r', i')	360, except u': 540
PTF1 J1632+3511	Keck-II/DEIMOS	2011 July 5[a]	Unknown	600ZD (600/7500)	900
PTF1 J2219+3135	Keck-I/LRIS	2011 November 25[a]	Quiescence	B: 400/3400, R: 400/7500	1200
...	P200/LFC	2012 November 22	Quiescence	Imaging (u', g', r', i')	300, except u': 600

[a]Indicates that this exposure (or the co-addition of the exposures) is shown in this paper.
P200/DBSP: Palomar 200-arcsec telescope with the Double Spectrograph (Oke & Gunn 1982).
Keck-I/LRIS: Keck-I 10-m telescope with the Low Resolution Imaging Spectrometer (Oke et al. 1995; McCarthy et al. 1998).
KPNO 4-m/RC: KPNO 4-m Mayall telescope with the RC Spectrograph.
NOT/ALFOSC: 2.5-m Nordic Optical Telescope with the Andalucia Faint Object Spectrograph and Camera.
P200/LFC: Palomar 200-arcsec telescope with the Large Format Camera.
Keck-II/DEIMOS: Keck-II 10-m telescope with the Deep Imaging Multi-Object Spectrograph (Faber et al. 2003).

used for measurements, and absolute calibration was done by comparing with SDSS measurements in the same filter.

2.2 Period analysis

For two of the systems, we attempted to measure the orbital period by looking for the 'S-wave' using the method in Nather, Robinson & Stover (1981). The short orbital periods of AM CVn systems require short exposures, and, for these faint systems, 5–10 h of time on a 8–10 m telescope. The S-wave is thought to be caused by the orbital motion of the accretion disc bright spot, formed by the impact of transferred mass hitting the disc (e.g. Warner 1995). For each spectrum obtained, we summed the flux for 1000 km s^{-1} on either side of the strongest lines and divided the two measurements. This set of ratios were analysed for each system using a Lomb–Scargle periodogram as implemented in Richards et al. (2011).

The verification of the orbital period was done in two ways. First, the strongest emission lines were co-added for each individual spectrum and converted into a trailed, phase-binned spectrum. This is essentially a two-dimensional representation with wavelength/velocity on one axis and time/phase on the other. In this image, we expect to see a sinusoidal S-wave from the hotspot on top of the disc emission as a result of Doppler shift. The particular lines used varied for each system.

To further verify the orbital period, we transformed the phase-binned spectrum into a Doppler tomogram (Marsh & Horne 1988).

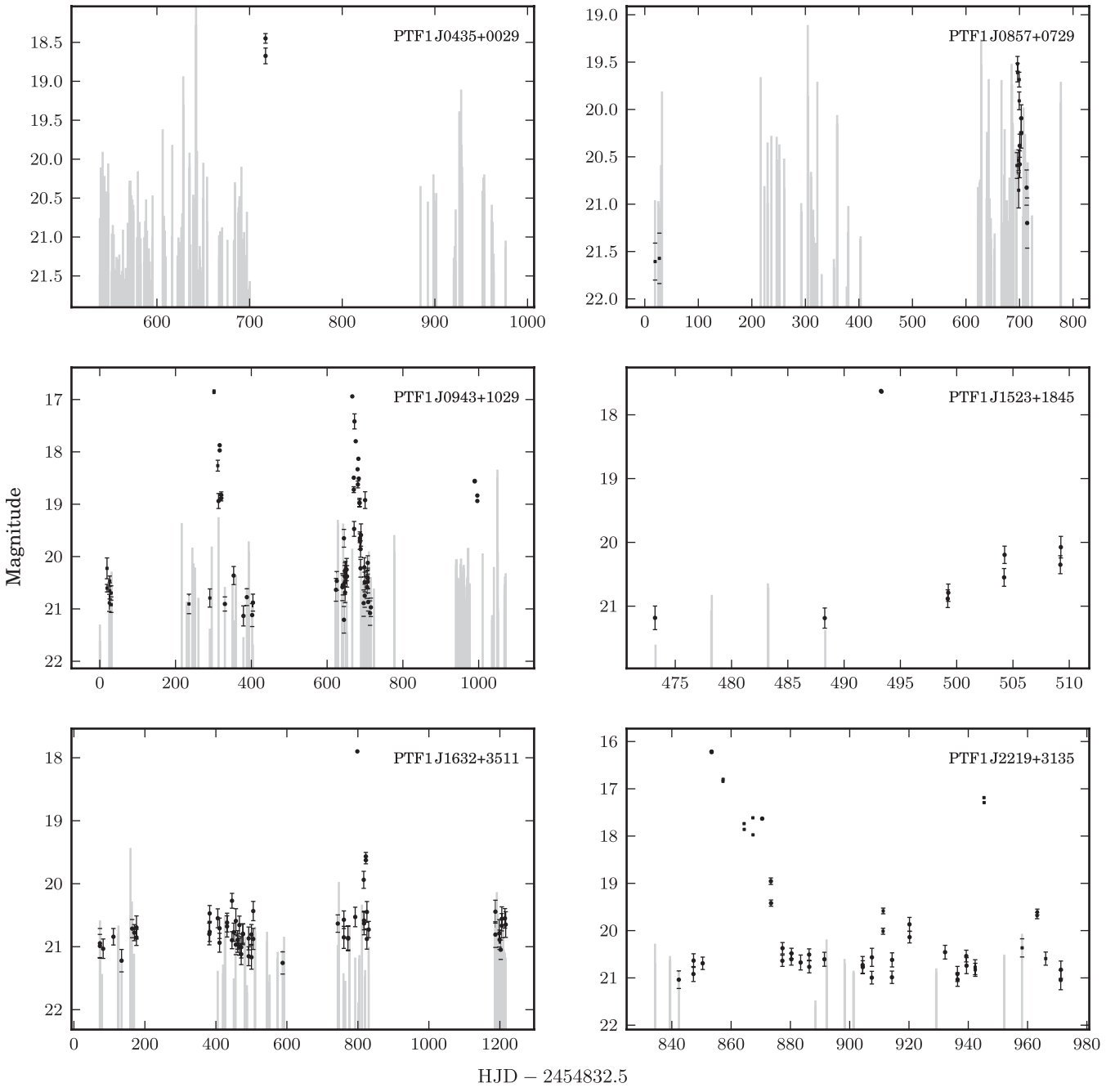

Figure 1. Light curves of all systems presented here. All data are from the PTF photometric pipeline. Error bars are shown for those observations with errors >5 per cent. Non-detections are indicated using the grey lines – the top of the line is the 3σ limiting magnitude as derived from the seeing, background and CCD characteristics. The dates shown are relative to 2009 January 1. All data taken for each system by the PTF are shown except for PTF1 J1523+1845, for which there were 12 prior non-detections to limiting magnitudes of ∼21 over the 400 d before the data shown. We do not differentiate between *R* and g' data here, although the vast majority are *R*.

Doppler tomograms are essential in the study of semi-detached systems since they concentrate orbital velocity variations in a single location on a velocity map. The phase, radial velocity, and intensity data were used to produce an image in (K_x, K_y) velocity space. (K_x, K_y) = (0, 0) is the location of the centre of mass. For semi-detached systems, the following four components are typically seen:

(i) *The accretor.* For AM CVn systems, the absorption line features of the accretor itself are masked by the emission lines from the accretion disc and thus not visible in the Doppler tomogram. However, a narrow emission line feature referred to as the 'central spike' is visible on some typically longer period systems and is believed to be on or near the accretor (see e.g. GP Com; Morales-Rueda et al. 2003). The extreme mass ratio of AM CVn systems results in the accretor having a low velocity.

(ii) The accretion disc will extend from a relatively low velocity corresponding to the Keplerian orbital velocity of the outer edge of the disc to the much higher Keplerian orbital velocity at the radius of the WD.

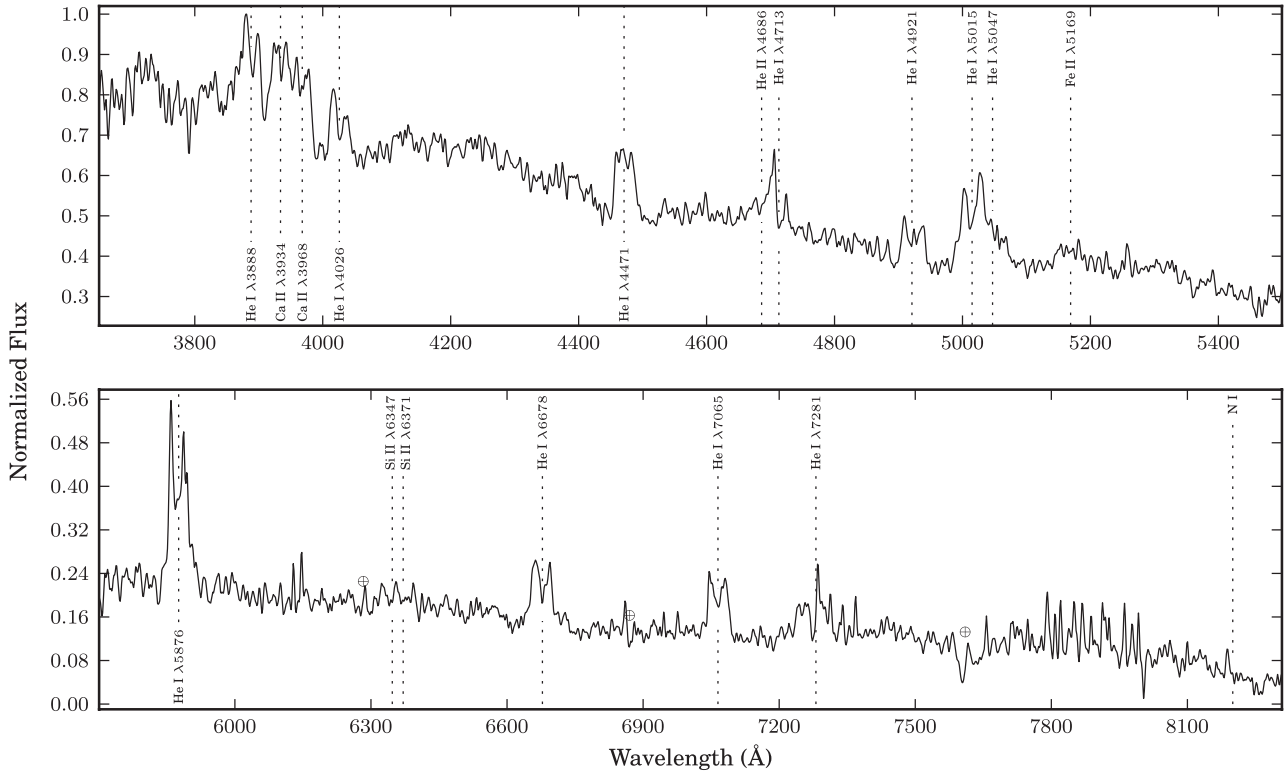

Figure 2. A spectrum of PTF1 J0435+0029 obtained from ∼4 h of co-added exposures of 2011 October 29.

(iii) The donor star will have a lower velocity than the outer edge of the accretion disc. From Keplerian orbital mechanics,

$$v_{\rm don} = \left(\frac{2\pi G}{P_{\rm orb}}\right)^{1/3} \sqrt{\frac{M_{\rm acc}}{(M_{\rm acc}+M_{\rm don})^{1/3}}},$$

where $v_{\rm don}$ is the velocity of the donor, G is the gravitational constant, $P_{\rm orb}$ is the orbital period of the system, $M_{\rm acc}$ is the mass of the accretor and $M_{\rm don}$ is the mass of the donor. If we set, for example, $M_{\rm acc} = 0.85\,{\rm M}_{\odot}$ and $M_{\rm don} = 0.035\,{\rm M}_{\odot}$, as found for the eclipsing AM CVn system SDSS J0926+3624 in Copperwheat et al. (2011), we find that $v_{\rm don} \approx 700\,{\rm km\,s^{-1}}$. However, the donor is typically not seen in AM CVn systems due to its much lower luminosity relative to the accretor and disc. The sole exception thus far is the 5.4 min orbital period system HM Cnc (Roelofs et al. 2010).

(iv) The hotspot is expected to be on the inner edge of the accretion disc on the Doppler tomogram, at a relatively constant velocity. The location relative to the accretor is dependent on the size of the disc, but, for longer period systems, is typically on the opposite side of the centre of mass in (K_x, K_y) space. The identification of a well-defined hotspot in the Doppler tomogram is a requirement to establish the orbital period (e.g. Roelofs et al. 2006b).

3 AM CVn SYSTEMS

We summarize the newly discovered AM CVn systems in Table 1. Hereafter, we will refer to all systems using the shorter PTF1 JHHMM+DDMM convention as opposed to their full coordinates.[2]

[2] Non-transient sources in PTF are identified using the conventional IAU name format in the PTF1 catalogue, a preliminary version of the final PTF catalogue. This is different from the PTF transient convention that identifies events by the year and a character sequence.

All observations are summarized in Table 2. The PTF light curves for all discovered systems are in Fig. 1. We determined that these systems are AM CVn systems based on the presence of helium, the lack of hydrogen, and the observed outbursts.

3.1 PTF1 J043517.73+002940.7

PTF1J0435+0029 was detected in outburst by the transient pipeline on 2011 February 16 and identified as a candidate of interest by the Galaxy Zoo Supernovae project (Smith et al. 2011). Only two detections were made as the field was not observed again until the following season. Follow-up classification spectra on 2011 March 10 and 2011 March 12 showed a mostly featureless continuum spectrum. However, a spectrum taken on 2011 March 26 showed helium emission lines consistent with those of known AM CVn systems.

On 2011 October 29, we obtained 5.18 h of phase-resolved spectroscopy. We present the co-added spectrum in Fig. 2. We analysed these data as described in Section 2.2 and present the periodogram of the flux ratios in Fig. 3. The periodogram shows a peak at 34.31 min, but one that is broad due to the short baseline. The uncertainty of period measurement was estimated using a simple Monte Carlo simulation. For each iteration of the simulation, we selected 105 exposures at random, allowing for repetition, and calculated the periodogram. We estimate the error to be 1.94 min, which is the standard deviation in the period estimates of 1000 such iterations. This is consistent with the full width at half-maximum (FWHM) of the peak, which is 1.75 min. The more complicated error estimate used for PTF1 J0943+1029 (see Section 3.3) could not be used here due to the lack of a strong signal.

We trailed, binned and folded the spectrum in an attempt to confirm the S-wave visually. This, as well as a Doppler tomogram,

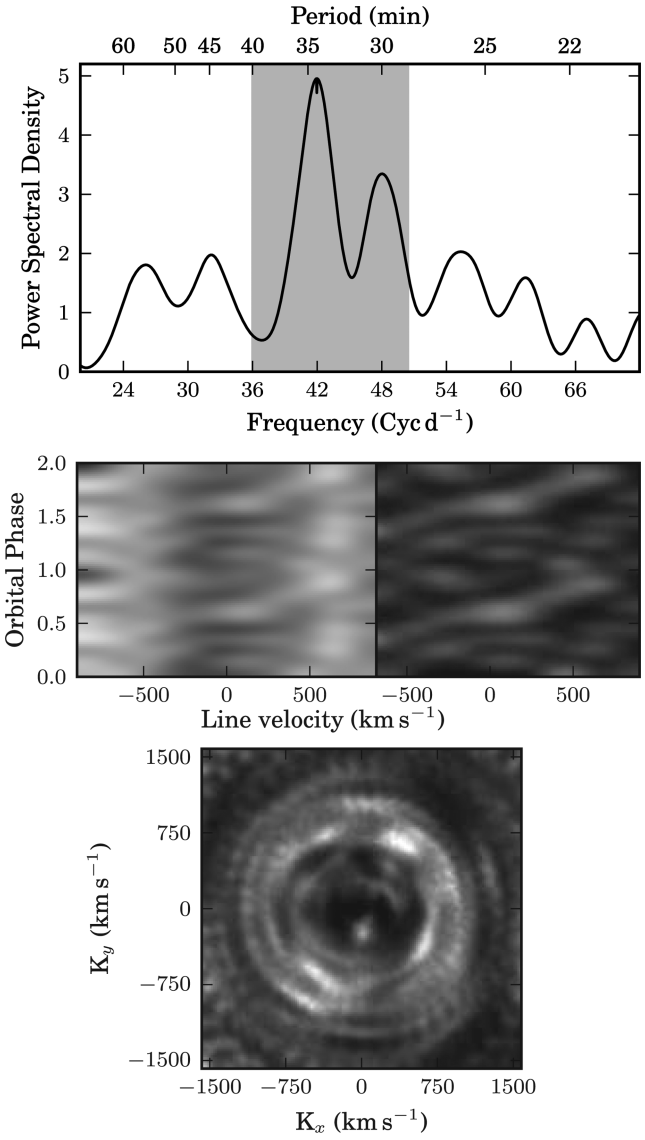

Figure 3. Top panel: periodogram of the co-added He I line flux ratios from 5.18 h of PTF1 J0435+0029 observations. The calculation of these flux ratios is described in Section 2.2. The He I lines at λλ3888, 4026, 4471 and 5015 were used to calculate the flux ratios for this system. The 3σ confidence interval is shaded. Middle panels: the binned, trailed spectra of PTF1 J0435+0029 using the co-added He I lines at λλ4026, 4471, 4713, 4921, 5015, 5875, 6678 and 7065 folded at 34.31 min. This corresponds to the peak of the periodogram. An arbitrary zero phase of HJD = 245 5863.910 02 was used, coinciding with the start of the observations. The version on the left-hand side retains the disc emission, while the version on the right-hand side removes the disc emission by subtracting the median of each column. Bottom panel: a Doppler tomogram of PTF1 J0943+1029 constructed from the same emission lines as the S-wave, plotted to highlight the peak believed to be the hotspot at (K_x, K_y) ≈ (380, 655) km s^{-1} (the upper right-hand part of the image). An arbitrary zero phase of HJD = 245 5863.910 02 was used, coinciding with the start of the observations.

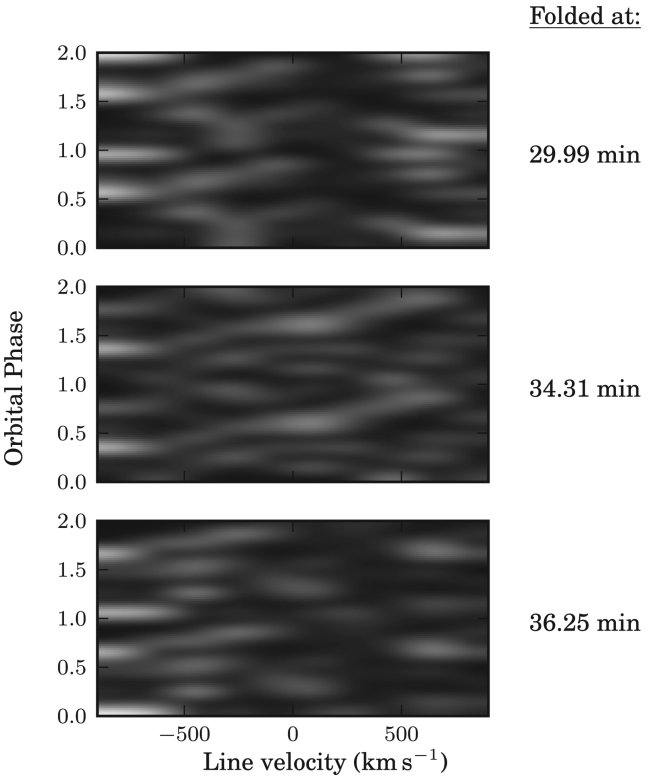

Figure 4. A comparison of the binned, trailed spectra of PTF1 J0435+0029 using the co-added He I lines at λλ4026, 4471, 4713, 4921, 5015, 5875, 6678 and 7065 folded, from the top to bottom, at 29.99, 34.31 and 36.25 min. These correspond to the second most significant peak of the periodogram, the proposed orbital period and the period at the upper end of the error estimate, respectively. An arbitrary zero phase of HJD = 245 5863.910 02 was used for all three plots, coinciding with the start of the observations. The median of each velocity bin was subtracted to remove the contribution from the accretion disc. Only the plot at 34.31 min, the proposed orbital period, shows a discernible S-wave; plots at other periods show noise and no signal.

is also presented in Fig. 3. Fig. 4 shows a comparison of the S-wave at the stated orbital period to those generated with two other example periods: 29.99 min and $P_{\rm orb}$ + 1.94 min. The former is the next highest peak on the periodogram. The latter is 1 standard deviation away from the highest peak and would not be expected to show any signal if the periodogram is valid. There is no S-wave present at the alternate periods, despite the relatively high peak at 32.99 min in the periodogram. Similar plots at other possible orbital periods likewise show no signs of an S-wave.

The proposed orbital period is in the same range as that of other known AM CVn systems with similar photometric behaviour. Levitan et al. (2011) and Ramsay et al. (2012) noted that systems with infrequent outbursts are associated with longer orbital periods. The outburst on 2011 February 16 was the only observed outburst of PTF1 J0435+0029 in PTF and there have been two recorded outbursts in the Catalina Real-Time Transient Survey (Drake et al. 2009) – one roughly coincidental with that observed by the PTF, and one ∼750 d prior. We thus expect the system to have an orbital period between ∼27 and ∼40 min (the longest observed period for outbursting systems). The faintness of the S-wave is not completely surprising since other systems (e.g. SDSS J0804+1616; Roelofs et al. 2009) have also been observed to have very weak S-waves at times.

We conclude our discussion of PTF1 J0435+0029 with some remarks on the characteristics of its spectrum. The spectrum of PTF1 J0435+0029 is particularly notable in this set of AM CVn systems for the absence of N I (see Fig. 2 and Table 3). This lack of N I likely points to a different donor composition from the other systems presented here. Specifically, the presence of N I has been

Table 3. Equivalent widths of prominent lines.

Line	PTF1 J0435+0029	PTF1 J0857+0729	PTF1 J0943+1029	PTF1 J1523+1845	PTF1 J2219+3135
Ca II 3933/3968	Blended with He	X	Blended with He	X	Blended with He
He I 4026	-4.6 ± 0.7	X	X	-3.7 ± 0.9	-5.1 ± 0.8
He I 4388	X	... [b]	-2.3 ± 0.3	-1.2 ± 0.5	-1.7 ± 0.2
He I 4471	-10.0 ± 0.7	-13 ± 5.1	-10.4 ± 0.3	-5.7 ± 0.7	-6.6 ± 0.2
He II 4685/4713	-6.4 ± 0.8	X	-9.6 ± 0.4	-5.7 ± 0.9	-3.5 ± 0.3
He I 4921	-7.9 ± 0.7	-10.6 ± 5.4	-1.6 ± 0.3	-2.5 ± 0.7	-4.8 ± 0.2
He I 5015/5047	-10.0 ± 0.6	-34.9 ± 5.9	-17.1 ± 0.4	-5.5 ± 0.8	-9.1 ± 0.2
He I 5875	-49.8 ± 2.0	-62.9 ± 5.6	-21.8 ± 0.6	-7.4 ± 0.7	X
He I 6678	-33.1 ± 2.0	-19.6 ± 5.6	-14.1 ± 0.6	-4.2 ± 0.8	-10.7 ± 0.2
He I 7065	-29.8 ± 1.9	-26.6 ± 5.1	-15.0 ± 0.7	... [b]	-15.1 ± 0.3
He I 7281	-28.4 ± 2.4	X	-9.3 ± 0.6	X	... [a]
Fe II 5169	-0.8 ± 0.7	X	-4.8 ± 0.3	... [b]	-9.8 ± 0.2
Si II 6347/6371	... [b]	X	-6.5 ± 0.7	-3.8 ± 0.6	-9.5 ± 0.3
N I 8184/8188/8200	X	... [c]	-7.8 ± 0.7	... [a]	-3.6 ± 0.9

Lines marked with an X indicate that this line is not detectable above the noise level of the spectrum obtained.
[a]Line present but contaminated with atmosphere.
[b]Line present but insufficient S/N to measure.
[c]Spectrum does not extend to this wavelength.

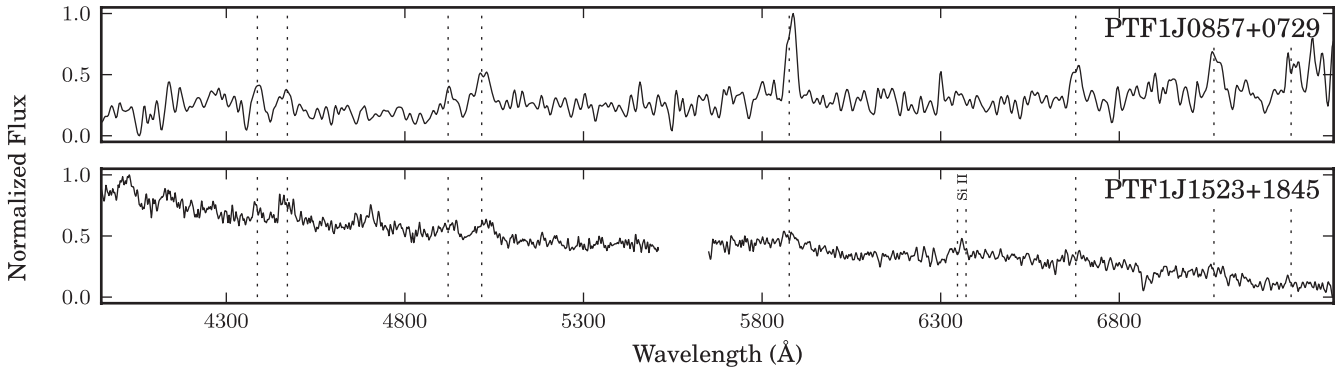

Figure 5. Spectra of PTF1 J0857+0729 and PTF1 J1523+1845 taken in outburst. Prominent He I lines at λλ4387, 4471, 4921, 5015, 5875, 6678, 7065 and 7281 are marked with the dashed lines, as well as Si II for PTF1 J1523+1845. The specific observations used are marked in Table 2. Spectra were Gaussian smoothed by 5 pixels. We particularly note the presence of emission lines and no absorption lines in both systems, something that has not been observed previously in AM CVn system outburst spectra.

linked to a highly enriched CNO cycle in He WD donors, whereas the abundance decreases in He-star donors because of α-capture on N (Nelemans et al. 2010). Thus, this system may have evolved from the He-star donor evolutionary track as opposed to the detached WD binary track.

3.2 PTF1 J085724.27+072946.7

PTF1 J0857+0729 was discovered in outburst by the transient pipeline on 2011 January 27. A classification spectrum taken on 2011 February 1 showed distinct helium emission lines, which were confirmed with a second spectrum the following night (see Fig. 5).

In CVs, the presence of emission lines in outburst is indicative of a high-inclination, and thus often eclipsing, system (e.g. Warner 1995). Previously, all AM CVn systems spectroscopically observed in outburst showed absorption lines (e.g. Roelofs et al. 2007b). We obtained a 2-h light curve at the P200 on 2011 November 30 (45 s exposure time; 24 s dead time) and another 2-h light curve at the NOT on 2012 February 28 (60 s exposure time; 5 s dead time) to search for eclipses. AM CVn systems are expected to have very short eclipses of the order of a minute (e.g. Copperwheat et al. 2011), so short exposures times are necessary.

The individual photometric measurements had errors of ∼3 and ∼5 per cent, respectively. Periodograms constructed from these light curves showed no significant period, although the light curves did show variability with an amplitude of 0.1–0.15 mag. Lack of data precludes a definitive determination, but this is consistent with the amplitude of periodic variability found in other quiescent AM CVn systems (e.g. Provencal et al. 1997). None of the photometric measurements was fainter than 0.1 mag below the median magnitude and thus we conclude that no eclipses were detected.

We next consider whether eclipses may have been missed due to dead time between exposures. We assume that the eclipse duration is 60 s with steep ingress and egress and a worst case scenario where the dead time is exactly in the middle of the eclipse. Given the possible variability observed and the short observing times, we define an eclipse to be a measurement at least 0.3 mag (2–3 times the variability) below the median. We calculate that in this worst case scenario, eclipses of $\gtrsim$1.0 mag should have been visible in the P200 data and eclipses of $\gtrsim$0.8 mag should have been visible in the NOT data. Thus, any eclipses missed are relatively shallow.

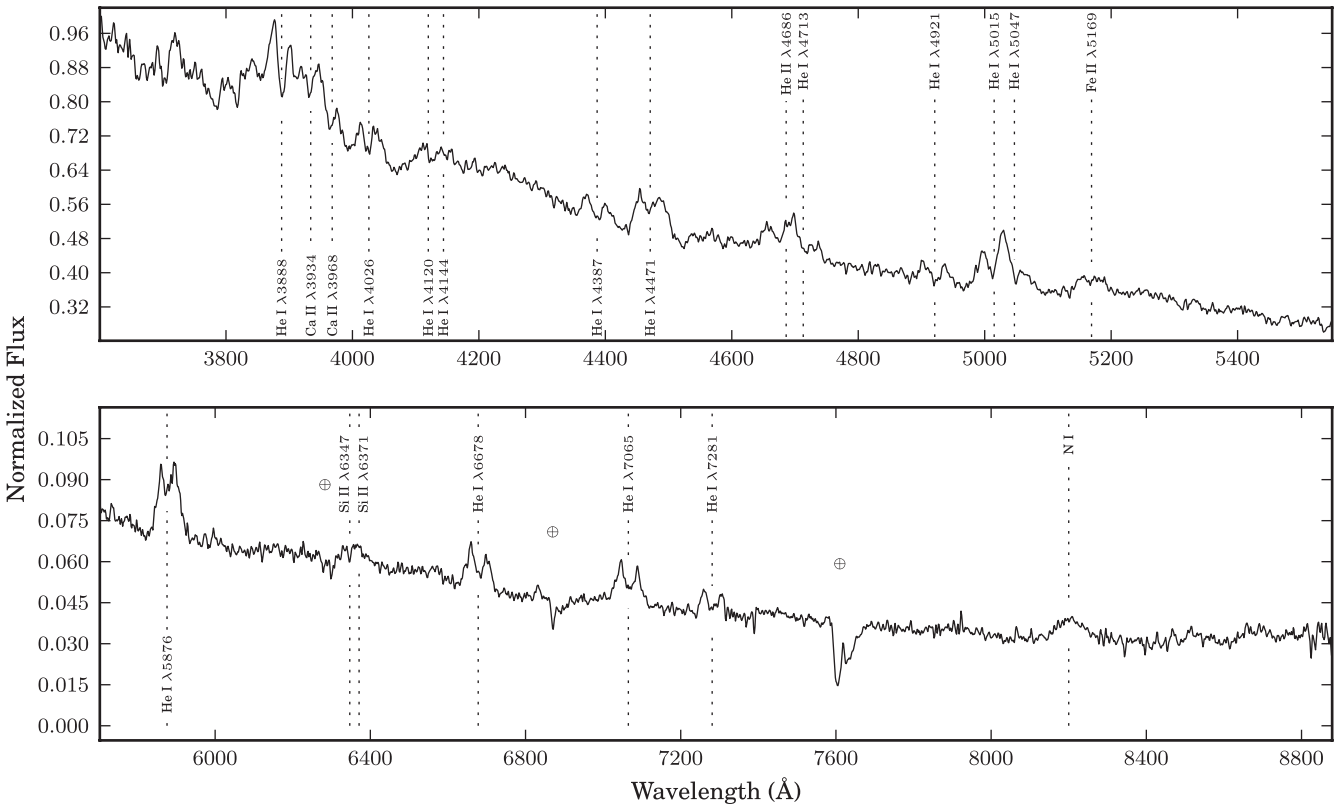

Figure 6. A spectrum of PTF1 J0943+1029 in quiescence. The blue (top panel) spectrum is a co-addition of the ∼4 h observed on 2011 December 25. The red (bottom panel) spectrum is a co-addition of the ∼1.5 h observed on 2011 December 31.

3.3 PTF1 J094329.59+102957.6

PTF1 J0943+1029 was discovered as part of the photometric data base search (see the light curve in Fig. 1). An initial classification spectrum showed strong helium emission lines. We obtained a total of 5.45 h of phase-resolved spectroscopy of PTF1 J0943+1029 on 2011 December 25 and 31 using Keck-I/LRIS. We present the co-added spectrum in Fig. 6.

These data were analysed for the orbital period. The peak of the periodogram is at 30.35 min (Fig. 7), and an S-wave and Doppler tomogram generated at this period show a strong signal (Fig. 8). The number of strong aliases adjacent to the peak frequency makes a good error estimate crucial.

To obtain an estimate of the error, we exploited the properties of the Doppler tomograms. As discussed in Section 2.2, the hotspot should be concentrated in a single spot on the Doppler tomogram. Hence, the correct orbital period should correspond to the Doppler tomogram with the sharpest hotspot. We define this to be the hotspot with the smallest FWHM, using a two-dimensional Gaussian model. We note that this method could not be used reliably for PTF1 J0435+0029 due to the much worse signal-to-noise ratio (S/N) in the data.

We calculated 1000 Doppler tomograms for periods between 27.2 and 33.5 min in ∼0.1 min steps (43–53 cycle d^{-1} in 0.1 cycle d^{-1} steps) and measured the FWHM of the hotspot in each using a two-dimensional Gaussian fit. To estimate the error, for each of 1000 iterations, we drew 100 FWHM measurements from the range of 46 to 50 cycle d^{-1} and fitted a parabola to the measurements. This limited range was required to eliminate inaccurate measurements due to multi-peak 'spots' outside this range that gave inaccurate, small FWHM measurements.

This simulation found a median period of 30.17 ± 0.65 min, within 1σ of the peak of the periodogram. We plot all FWHMs and the best fit using all points in Fig. 7. The error estimate of this simulation is consistent with a visual inspection of S-waves and Doppler tomograms around the peak of the periodogram. Given the error and the visual representations of the orbit in Fig. 8, we conclude that the median period from this simulation is the orbital period of the system.

3.4 PTF1 J152310.71+184558.2

PTF1J1523+1845 was discovered in outburst on 2010 July 7 as part of the transient search. Spectra taken on 2010 July 7 and 8 showed He I emission lines (see Fig. 5). This makes it the second known outbursting AM CVn system to exhibit emission lines in outburst. Extensive follow-up on this system was not performed, due to its faint nature ($g' > 23$).

3.5 PTF1 J163239.39+351107.3

PTF1 J1632+3511 was discovered in outburst on 2011 May 11 and a spectrum was obtained on 2011 July 5. This source is extremely faint ($g' \approx 23$) and is located adjacent to a significantly brighter galaxy. We present the spectrum in Fig. 9. The spectrum shows He I λ5875 emission, possible He I λ6678 and He II λ4686 emission, and no trace of H lines. We exclude it as a possible supernova from the He I lines at $z = 0$. Based on the evidence, we conclude that PTF1 J1632+3511 is a likely AM CVn system, but a higher S/N spectrum is required before this can be established with certainty.

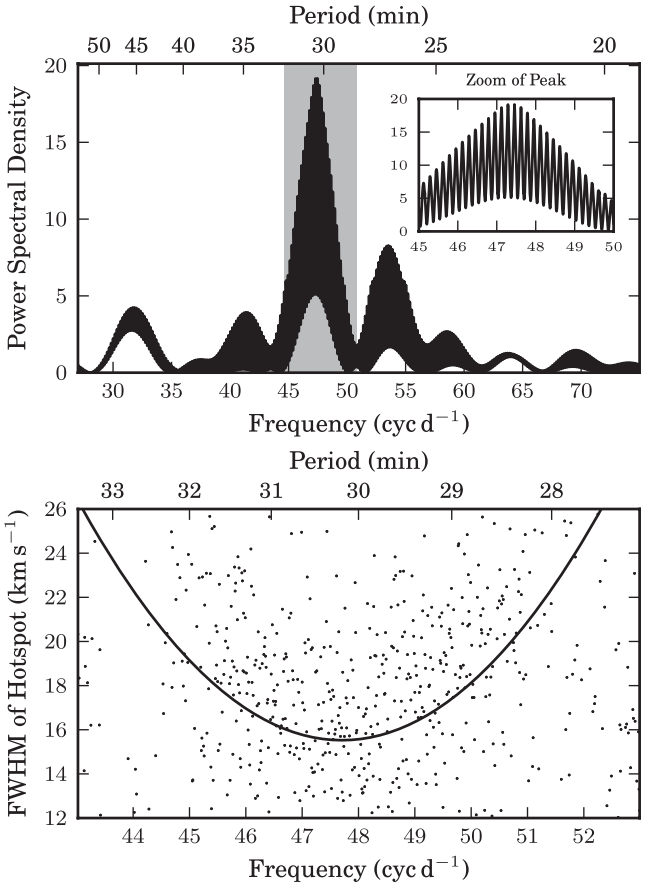

Figure 7. Top panel: periodogram of the flux ratios of PTF1 J0943+1029. There are no strong peaks outside the frequency range shown here. The peak is at 30.35 min. The He I lines at λλ3888, 4026, 4471 and 5015 were used to calculate the flux ratios for this system. The shaded region represents the 3σ confidence interval around the proposed orbital period. Bottom panel: the FWHMs of the hotspots in 1 000 Doppler maps calculated at a range of periods. The solid line is the best fit of a quadratic equation. Its minimum of 30.17 min is within 1σ of the peak of the periodogram.

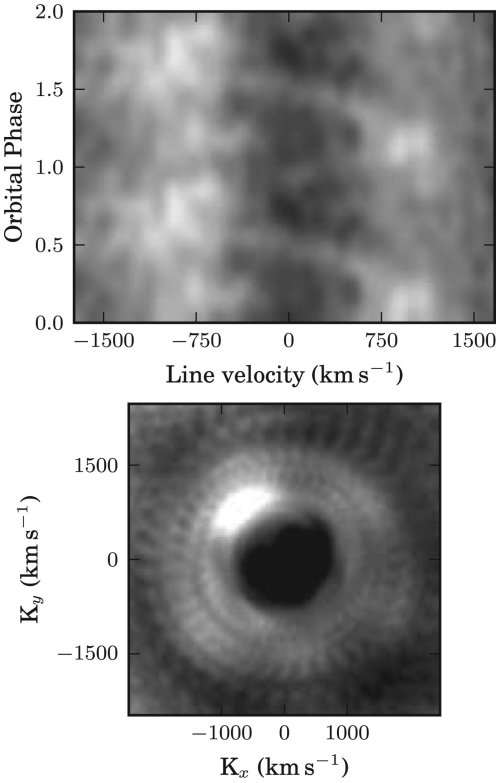

Figure 8. Top panel: the S-wave used to visually confirm the period of PTF1 J0943+1029. The He I lines at λλ3888, 4026, 4471, 4713, 4921 and 5015 and the He II line at λ4686 were folded at a period of 30.35 min to generate the image. The S-wave was phase-binned into 10 bins with a zero phase of HJD = 245 5920.962. Bottom panel: Doppler tomogram of PTF1 J0943+1029 using the He I λλ4027, 4471, 4713, 4921 and 5015 and He II λ4685 lines. The zero phase here is the same as for the S-wave.

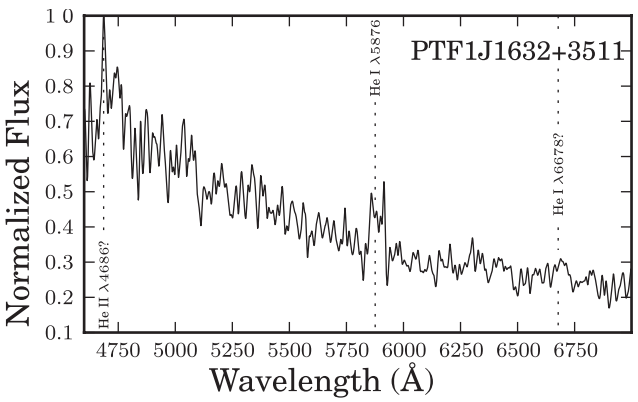

Figure 9. Classification spectrum of PTF1 J1632+3511 taken on 2011 July 5. The system is assumed to be either in or near quiescence. The closest PTF photometric measurement on 2011 July 11 has no detection to a limiting magnitude of 20.67. The poor quality of the spectrum precludes us from classifying this as an AM CVn system. However, after Gaussian smoothing by 10 pixels we can identify He I λ5875 emission, possible He I λ6678 and He II λ4686 emission, and no evidence of H.

3.6 PTF1 J221910.09+313523.1

PTF1 J2219+3135 was discovered as part of the photometric data base search (see Fig. 1 for the light curve and Fig. 10 for the identification spectrum). The relatively low quality identification spectrum has a particularly interesting set of lines. Specifically, several lines redwards of Fe II λ5169 at λ5276 and λ5317 have only been observed in V406 Hya (Roelofs et al. 2006a) ($P_{\rm orb}$ = 33.8 min) and SDSS J0804+1616 (Roelofs et al. 2009) ($P_{\rm orb}$ = 44.5 min). These may also be Fe II, but such lines are unusual. Note that unique identification of weak features is made more difficult due to the large width of the lines due to Doppler broadening of the rotating accretion disc.

4 DISCUSSION

4.1 Spectral features

We present equivalent widths for lines in each of the five systems presented in Table 3. In this section, we compare the features of the systems with relatively high S/N: PTF1 J0435+0029, PTF1 J0943+1029 and PTF1 J2219+3135. As expected, the spectra of the systems in this sample show signs of having shorter orbital periods than those detected in the SDSS. Particularly, we note the lack or relative weakness of the absorption wings surrounding the He emission lines. These absorption wings are from the WD primary

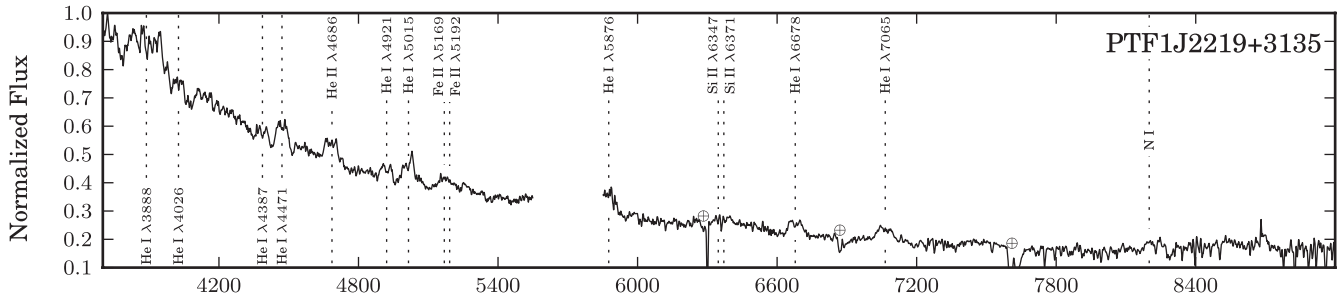

Figure 10. Classification spectrum of PTF1 J2219+3135 taken in quiescence. The prominent He and metal lines are marked (see Section 4.1).

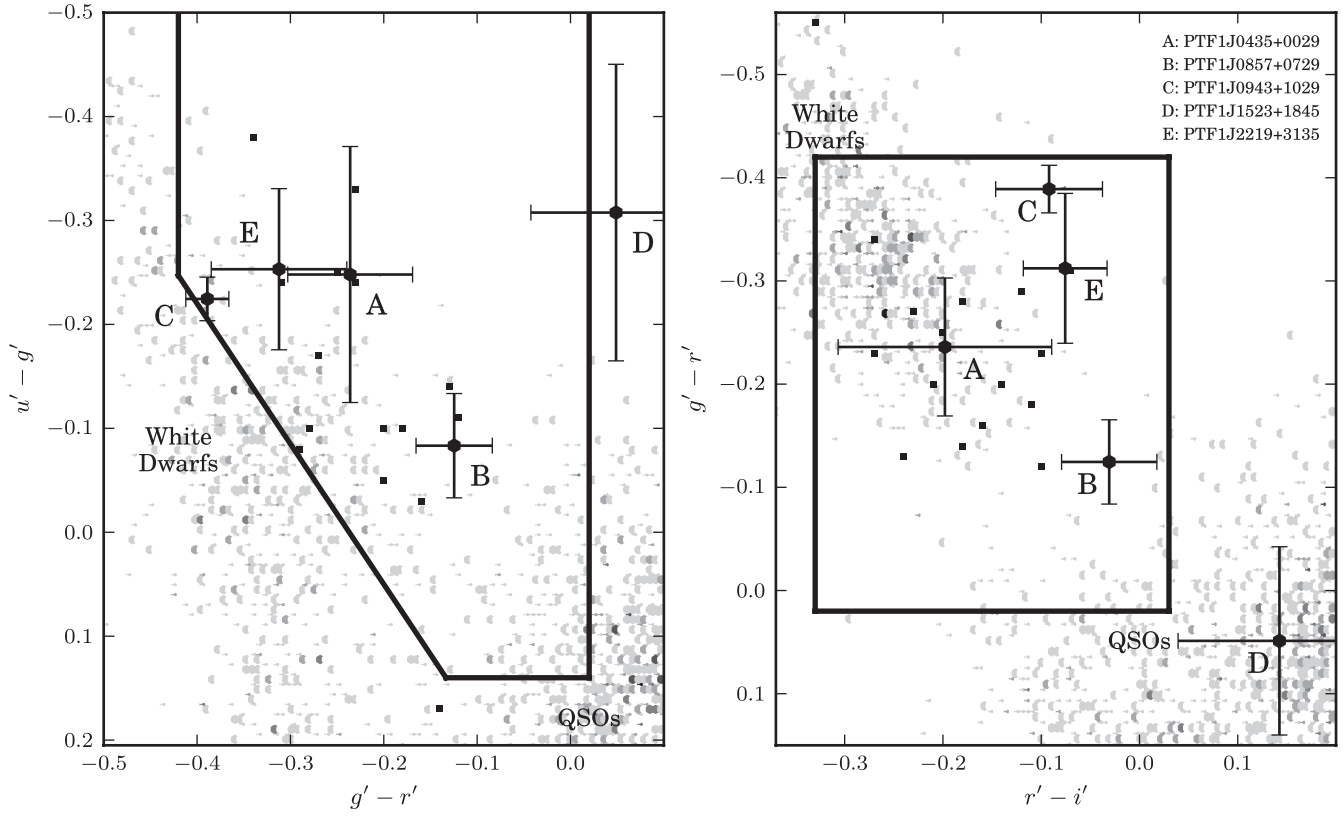

Figure 11. The colour–colour diagrams for AM CVn systems, including background SDSS-detected systems. AM CVn systems are marked as the black squares. Those labelled with a letter and with error bars are from this paper; those without are previously known systems with SDSS colours. The shaded areas indicate the density of the background systems – darker areas indicate a denser area in colour–colour space. The lines delineate the colour cut from Roelofs et al. (2009). We have corrected for extinction in the same way as Roelofs et al. (2009), but note that the distances to AM CVn systems are relatively small (Roelofs et al. 2007a) and thus the reddening is likely overestimated (Schlegel, Finkbeiner & Davis 1998; Roelofs et al. 2009). The PTF-discovered systems tend to lie close to the colour cut, but their exact position is uncertain due to large error bars.

and are expected to be less visible in shorter period systems if the mass transfer rate monotonously decreases with increasing orbital period, since this will create a relatively luminous accretion disc with respect to the luminosity of the accretor. We also see the presence of Ca II H&K in all three systems, which has been seen in shorter period systems such as V406 Hya (Roelofs et al. 2006a), but is less prevalent in longer period systems (those with $P_{\rm orb} >$ 50 min; Roelofs et al. 2005; Kupfer et al., in preparation).

Of particular interest for the general study of AM CVn systems is the identification of the donor and therefore the evolutionary history of these systems. Marsh, Horne & Rosen (1991) predicted the Si II emission at λ6346 and λ6371 and Fe II emission at λ5169 to be the strongest lines in helium-dominated, optically-thin accretion discs. They will be important to determine the initial metallicity in follow-up work as iron and silicon are not supposed to be affected by nuclear synthesis processes in AM CVn systems. Those features are well observed in other outbursting AM CVn systems, including V406 Hya (Roelofs et al. 2006a) and CP Eri (Groot et al. 2001). Here, we find the presence of Si II and Fe II in all three systems. However, as noted earlier, N I is uniquely missing in PTF1 J0435+0029, indicating the donor is more likely to have evolved from a He star. PTF1 J0943+1029 and PTF1 J2219+3135, on the other hand, are more likely to have a He WD as the donor star.

4.2 Comparison of system colours

The release of the SDSS data revolutionized the study of AM CVn systems. Initially, seven systems were discovered via a search for

He emission lines in the SDSS data base (Anderson et al. 2005, 2008; Roelofs et al. 2005). Subsequently, a spectroscopic survey of a colour-selected sample from SDSS was carried out and six more systems were found (Roelofs et al. 2009; Rau et al. 2010; Carter et al. 2013). However, both these studies have used colours to select systems for spectroscopic observation. In the case of the general SDSS survey, various criteria are used to select follow-up targets, while the dedicated AM CVn search used a colour cut based on the colours of known AM CVn systems.

The sample here, together with PTF1 J0719+4858 presented by Levitan et al. (2011), is unique as the first sample of AM CVn systems discovered systematically by their large-amplitude photometric variability as opposed to their spectral characteristics (and equivalently colours). It thus allows us to consider the completeness of the colour-selection criteria developed in Roelofs et al. (2009).

We note that these criteria target only quiescent systems since the spectra and colours of AM CVn systems do change during outbursts. Given that the SDSS survey is expected to be most sensitive to longer period systems and that these are believed to make up the vast majority of the population, this is a valid assumption. However, although our colours of PTF-discovered systems are from the quiescent states, our better sensitivity to shorter period systems may result in slightly different colours.

The quiescent magnitudes in each filter were presented in Table 1 and we plot the colours of our sources, together with known AM CVn systems and background sources, in Fig. 11. The colours of the PTF-discovered systems are from the quiescent state; those of previously known systems are determined from the SDSS photometry and may or may not be in quiescence. However, given that these are all longer period systems, it is highly likely that almost all are in quiescence. We do not include PTF1 J1635+3511 in this plot since it is only a candidate. Additionally, it is likely contaminated with the nearby galaxy, especially at the redder wavelengths.

We find that the PTF-discovered systems generally fall within the colour cut. One system, PTF1 J1523+1845, does show colours outside the colour cut, but, given its faintness, additional measurements should be made to verify this. Given these results, we urge caution in narrowing the colour cut, as suggested by Carter et al. 2013, to avoid missing redder AM CVn systems. However, both additional systems and further measurements are necessary before concluding whether outburst identification is sensitive to a population substantially different from the SDSS colour-selected sample.

5 CONCLUSIONS

We present five new AM CVn systems and one new AM CVn candidate, which were identified by their characteristic He I and He II emission lines and lack of H. We further present spectroscopic measurements of three of these systems, finding their orbital periods to be consistent with other AM CVn systems. Two of the systems presented here have the unique characteristic of strong emission lines while in outburst, often seen in eclipsing CV systems. We tested whether one of these systems is eclipsing but did not find evidence to support this hypothesis. Finally, we compared the spectroscopic and photometric features of these systems to other known AM CVn systems.

ACKNOWLEDGMENTS

We thank Sagi Ben-Ami, Yi Cao, Brad Cenko, Avishay Gal-Yam, Assaf Horesh, Mansi Kasliwal, Thomas Matheson, Kunal Mooley and Robert Quimby for help in obtaining observations and reducing data. We thank Kevin Rykoski and Carolyn Heffner at the Palomar Observatory for developing the fast cadence mode on the LFC instrument. Part of this work was performed by TAP while at the Aspen Center for Physics, which is supported by NSF Grant #1066293. PJG thanks the California Institute of Technology for its hospitality during his sabbatical stay.

Observations obtained with the Samuel Oschin Telescope at the Palomar Observatory as part of the Palomar Transient Factory project, a scientific collaboration between the California Institute of Technology, Columbia University, Las Cumbres Observatory, the Lawrence Berkeley National Laboratory, the National Energy Research Scientific Computing Center, the University of Oxford and the Weizmann Institute of Science. Some of the data presented herein were obtained at the W. M. Keck Observatory, which is operated as a scientific partnership among the California Institute of Technology, the University of California and the National Aeronautics and Space Administration. The Observatory was made possible by the generous financial support of the W. M. Keck Foundation. The authors wish to recognize and acknowledge the very significant cultural role and reverence that the summit of Mauna Kea has always had within the indigenous Hawaiian community. We are most fortunate to have the opportunity to conduct observations from this mountain. Based in part on observations made with the Nordic Optical Telescope, operated on the island of La Palma jointly by Denmark, Finland, Iceland, Norway and Sweden, in the Spanish Observatorio del Roque de los Muchachos of the Instituto de Astrofisica de Canarias. The data presented here were obtained in part with ALFOSC, which is provided by the Instituto de Astrofisica de Andalucia (IAA) under a joint agreement with the University of Copenhagen and NOTSA. This research has made use of NASA's Astrophysics Data System.

REFERENCES

Anderson S. F. et al., 2005, AJ, 130, 2230
Anderson S. F. et al., 2008, AJ, 135, 2108
Bildsten L., Shen K. J., Weinberg N. N., Nelemans G., 2007, ApJ, 662, L95
Carter P. et al., 2013, MNRAS, 429, 2143
Copperwheat C. M. et al., 2011, MNRAS, 410, 1113
Drake A. J. et al., 2009, ApJ, 696, 870
Faber S. M. et al., 2003, in Iye M., Moorwood A. F. M., eds, SPIE Conf. Ser. Vol. 4841, Instrument Design and Performance for Optical/Infrared Ground-based Telescopes. SPIE, Bellingham, p. 1657
Fontaine G. et al., 2011, ApJ, 726, 92
Groot P. J., Nelemans G., Steeghs D., Marsh T. R., 2001, ApJ, 558, L123
Horne K., 1986, PASP, 98, 609
Jha S., Garnavich P., Challis P., Kirshner R., Berlind P., 1998, IAU Circ., 6983, 1
Kato T., Nogami D., Baba H., Hanson G., Poyner G., 2000, MNRAS, 315, 140
Law N. M. et al., 2009, PASP, 121, 1395
Levitan D. et al., 2011, ApJ, 739, 68
McCarthy J. K. et al., 1998, in D'Odorico S., ed., Proc. SPIE Vol. 3355, Optical Astronomical Instrumentation. SPIE, Bellingham, p. 81
Marsh T. R., 1989, PASP, 101, 1032
Marsh T. R., Horne K., 1988, MNRAS, 235, 269
Marsh T. R., Horne K., Rosen S., 1991, ApJ, 366, 535
Morales-Rueda L., Marsh T. R., Steeghs D., Unda-Sanzana E., Wood J. H., North R. C., 2003, A&A, 405, 249
Nather R. E., Robinson E. L., Stover R. J., 1981, ApJ, 244, 269
Nelemans G., 2005, in Hameury J.-M., Lasota J.-P., eds, ASP Conf. Ser. Vol. 330, The Astrophysics of Cataclysmic Variables and Related Objects. Astron. Soc. Pac., San Francisco, p. 27

Nelemans G., Portegies Zwart S. F., Verbunt F., Yungelson L. R., 2001, A&A, 368, 939
Nelemans G., Yungelson L. R., Portegies Zwart S. F., 2004, MNRAS, 349, 181
Nelemans G., Yungelson L. R., van der Sluys M. V., Tout C. A., 2010, MNRAS, 401, 1347
Nissanke S., Vallisneri M., Nelemans G., Prince T. A., 2012, ApJ, 758, 131
Ofek E. O., Frail D. A., Breslauer B., Kulkarni S. R., Chandra P., Gal-Yam A., Kasliwal M. M., Gehrels N., 2011, ApJ, 740, 65
Ofek E. O. et al., 2012, PASP, 124, 62
Oke J. B., Gunn J. E., 1982, PASP, 94, 586
Oke J. B. et al., 1995, PASP, 107, 375
Provencal J. L. et al., 1997, ApJ, 480, 383
Ramsay G., Barclay T., Steeghs D., Wheatley P. J., Hakala P., Kotko I., Rosen S., 2012, MNRAS, 419, 2836
Rau A. et al., 2009, PASP, 121, 1334
Rau A., Roelofs G. H. A., Groot P. J., Marsh T. R., Nelemans G., Steeghs D., Salvato M., Kasliwal M. M., 2010, ApJ, 708, 456
Richards J. W. et al., 2011, ApJ, 733, 10
Roelofs G. H. A., Groot P. J., Marsh T. R., Steeghs D., Barros S. C. C., Nelemans G., 2005, MNRAS, 361, 487
Roelofs G. H. A., Groot P. J., Marsh T. R., Steeghs D., Nelemans G., 2006a, MNRAS, 365, 1109
Roelofs G. H. A., Groot P. J., Nelemans G., Marsh T. R., Steeghs D., 2006b, MNRAS, 371, 1231
Roelofs G. H. A., Groot P. J., Benedict G. F., McArthur B. E., Steeghs D., Morales-Rueda L., Marsh T. R., Nelemans G., 2007a, ApJ, 666, 1174
Roelofs G. H. A., Groot P. J., Nelemans G., Marsh T. R., Steeghs D., 2007b, MNRAS, 379, 176
Roelofs G. H. A., Nelemans G., Groot P. J., 2007c, MNRAS, 382, 685
Roelofs G. H. A. et al., 2009, MNRAS, 394, 367
Roelofs G. H. A., Rau A., Marsh T. R., Steeghs D., Groot P. J., Nelemans G., 2010, ApJ, 711, L138
Schlegel D. J., Finkbeiner D. P., Davis M., 1998, ApJ, 500, 525
Smak J., 1967, Acta Astron., 17, 255
Smith A. M. et al., 2011, MNRAS, 412, 1309
Solheim J., 2010, PASP, 122, 1133
van Dokkum P. G., 2001, PASP, 113, 1420
Warner B., 1995, Cataclysmic Variable Stars. Cambridge Univ. Press, Cambridge
Webbink R. F., 1984, ApJ, 277, 355
Wood-Vasey W. M., Aldering G., Nugent P., Li K., 2003, IAU Circ., 8077, 1

This paper has been typeset from a TEX/LATEX file prepared by the author.